

Tuning the probability of defect formation via substrate strains in $\text{Sr}_2\text{FeMoO}_6$ films

Waheed A. Adeagbo,^{1,*} Martin Hoffmann,^{2,†} Arthur Ernst,^{2,3} Wolfram Hergert,¹ Minnamari Saloaro,⁴ Petriina Paturi,⁴ and Kalevi Kokko^{5,6}

¹*Institute of Physics, Martin Luther University Halle-Wittenberg, Von-Seckendorff-Platz 1, 06120 Halle, Germany*

²*Institute for Theoretical Physics, Johannes Kepler University Linz, Altenberger Straße 69, 4040 Linz, Austria*

³*Max Planck Institute of Microstructure Physics, Weinberg 2, 06120 Halle, Germany*

⁴*Wihuri Physical Laboratory, Department of Physics and Astronomy, University of Turku, FI-20014 Turku, Finland*

⁵*Department of Physics and Astronomy, University of Turku, FIN-20014 Turku, Finland*

⁶*Turku University Centre for Materials and Surfaces (MatSurf), Turku, Finland*

(Dated: April 20, 2022)

Since oxide materials like $\text{Sr}_2\text{FeMoO}_6$ are usually applied as thin films, we studied the effect of biaxial strain, resulting from the substrate, on the electronic and magnetic properties and, in particular, on the formation energy of point defects. From our first-principles calculations, we determined that the probability of forming point defects – like vacancies or substitutions – in $\text{Sr}_2\text{FeMoO}_6$ could be adjusted by choosing a proper substrate. For example, the amount of anti-site disorder can be reduced with compressive strain in order to obtain purer $\text{Sr}_2\text{FeMoO}_6$ as needed for spintronic applications, while the formation of oxygen vacancies is more likely for tensile strain, which improves the functionality of $\text{Sr}_2\text{FeMoO}_6$ as a basis material of solid oxide fuel cells. In addition, we were also able to include the oxygen partial pressure in our study by using its thermodynamic connection with the chemical potential. Strontium vacancies become for example more likely than oxygen vacancies at a pressure of 1 bar. Hence, this degree of freedom might offer in general another potential method for defect engineering in oxides besides, e.g., experimental growth conditions like temperature or gas pressure.

I. INTRODUCTION

Lattice imperfections like point defects can be crucial for the functionality of novel materials. They can destroy desired properties but might also improve or even just allow new functionalities. A good example is the double perovskite material $\text{Sr}_2\text{Fe}_{1+x}\text{Mo}_{1-x}\text{O}_{6-\delta}$, where x symbolizes non-stoichiometry at the B/B' site and δ oxygen-deficiency (general formula $A_2BB'O_6$). It is a versatile material, which is throughout literature considered for several potential applications.

For example, the half-metallic character of $\text{Sr}_2\text{FeMoO}_6$ (SFMO), which is experimentally observed as promising high spin polarization [1], is a highly desired property in order to access spintronics [2, 3]. Besides, SFMO shows a low-field magnetoresistance response, a magnetic transition above ambient temperatures [4], and a high magnetic moment per functional unit in a range of $2.2\mu_B/\text{f.u.}$ to $3.9\mu_B/\text{f.u.}$ [5–8]. Nevertheless, a successful utilization of SFMO is still problematic, since the theoretical predicted half-metallicity [9], which is one requirement of its high spin polarization, is usually diminished or even lost in thin film samples of $\text{Sr}_2\text{FeMoO}_6$ [10–13]. These deterioration effect was attributed to doping, defects, grain boundaries, or parasitic phases, so that, e.g., the saturation magnetization becomes strongly reduced compared with its theoretically expected value. The latter should be $4\mu_B/\text{f.u.}$ arising from the spin quantum number of $S = 5/2$ of the Fe^{3+} ions and the antiparallel cou-

pled electrons with $S = 1/2$ from the Mo^{5+} ions [9]. It was verified in many theoretical studies, which shed light upon the microscopic origins of the magnetic properties of SFMO and their alterations [14–20]. While oxygen vacancies – a common observation in transition metal oxides – seem not to interfere with the spin polarization of SFMO [13, 20–22], the stoichiometry preserving exchange of B and B' atoms, so-called antisite disorder (ASD), can strongly reduce the saturation magnetization, the spin polarization [21–23], the magneto-transport properties [24, 25] or might even influence long range magnetic ordering [26, 27]. Hence, a synthesis of $\text{Sr}_2\text{FeMoO}_6$ samples is rather difficult because of a non-negligible concentration of defects. Therefore, there is a strong desire to control the amount of defects in $\text{Sr}_2\text{FeMoO}_6$ samples [11, 13].

On the other hand, the easy formation of oxygen vacancies in $\text{Sr}_2\text{FeMoO}_6$ makes it a good candidate as mixed ionic electronic conductor in solid oxide fuel cells (SOFC) [20, 28]. Experimental studies investigate its potential as anodes with a non-stoichiometric ratio between Fe and Mo [29, 30], while theoretical studies calculate the oxygen diffusion [31] or the formation energy of oxygen vacancies in bulk $\text{Sr}_2\text{FeMoO}_6$ [20].

Both applications utilize thin films of SFMO [13, 32], where the substrate might cause epitaxial biaxial strain – another factor deteriorating the desired properties of the SFMO film [33]. Although very large biaxial strains could theoretically induce a spin transition in bulk SFMO [34], our recent study revealed not only that a compressive biaxial strain $\sim 1\%$ at SrTiO_3 substrates does not show any significant direct impact on the magnetic properties of SFMO [13], but also that the amount of ASD and oxy-

* waheed.adeagbo@physik.uni-halle.de

† martin.hoffmann@jku.at

gen vacancies is reduced compared to the observed defect concentrations in the SFMO bulk target from which the films were grown [13].

This increase of defect formation probabilities was an interesting experimental finding. Hence, we want to study the role of biaxial strain in SFMO further in more detail. In particular, oxygen vacancies are one way for various oxides to compensate tensile strain, since the observed chemical expansion can accommodate parts of the strain [35, 36]. It could mean therefore potentially room temperature magnetism for SFMO thin films due to tensile biaxial strain because oxygen vacancies were shown to increase the Curie temperature in SFMO as well [37].

However, other point defect than oxygen vacancies were only rarely discussed in literature on strained oxide materials. We carried out density-functional theory (DFT) calculations in order to study systematically the structural and magnetic properties of SFMO including various point defects under the influence of biaxial strain, in particular, ASD and other vacancies. We observe strong variations of formation energies up to 1 eV depending on the kind of considered defect allowing for potential defect engineering with the decision for a particular substrate.

II. TECHNICAL DETAILS

Our calculations are performed using the Vienna *ab initio* simulation package (VASP) [38, 39]. While we present here only setup information, which are deviating from a standard VASP setup used, e.g., in previous theoretical studies on SFMO [20, 22], we provide further numerical details and parameters in the Supplemental Material [40].

We used in our calculations the tetragonal unit cell containing two functional units (f.u.) of $\text{Sr}_2\text{FeMoO}_6$ (Figs. 1a and 1b) and a supercell comprising 8 f.u. of $\text{Sr}_2\text{FeMoO}_6$ – in total 80 atoms (Figs. 1c and 1d). Both structures stabilize after numerical relaxation in the space group $I4/m$, which is in agreement with experimental observations and shows oxygen octahedra, which rotate only slightly in the $x-y$ plane and remain static otherwise (Fig. 1). The Fe octahedra are rotated clockwise by $\beta = 7.43^\circ$ while the Mo octahedra rotate counter clockwise.

Former theoretical studies [19, 20, 22, 34] discuss correlation corrections GGA+ U as the crucial factor in order to obtain a total magnetic moment of $4.0\mu_B/\text{f.u.}$, but we will show below that this is also achieved with the fixed spin moment (FSM) method [41, 42] and a GGA functional alone. Besides, the band gap in the spin up channel obtained within the GGA+ U approach is too wide compared with experimental measured values of 0.5 eV, 1.3 eV [7, 40, 43].

The FSM method allows instead to treat the total energy as an explicit function of the magnetization. It was in particular important for regions of large compressive

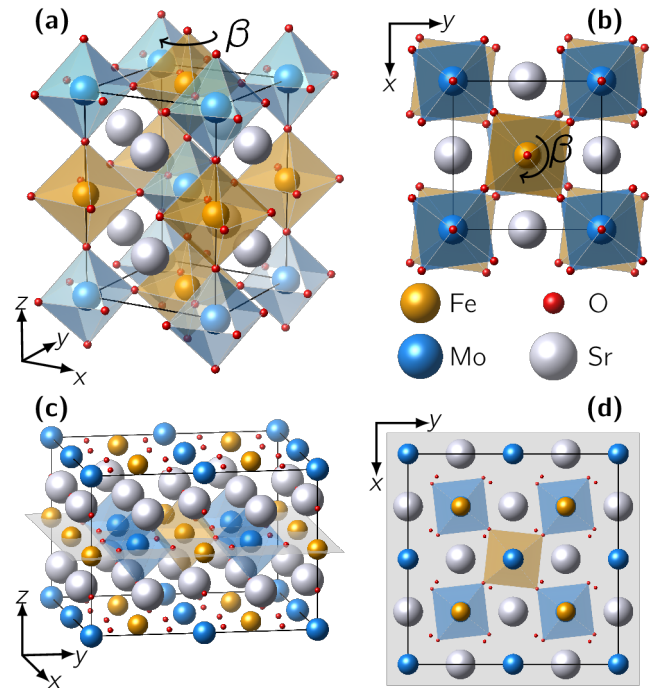


FIG. 1. (Color online) Considered lattice structures of $\text{Sr}_2\text{FeMoO}_6$: (a) Tetragonal unit cell with $I4/m$ symmetry visualizing the octahedral environment of Fe and Mo formed by the oxygen atoms with colored polyhedra. (b) Top view showing the octahedra rotation denoted as β and counted in clockwise direction for the Fe ion octahedron. (c) Side view of the $2 \times 2 \times 1$ supercell with 8 f.u. used for the defect calculations. (d) Top view of the supercell in (c) from the gray xy layer downwards.

or tensile strain where the total energy landscape can be strongly varied and where it becomes more difficult to ascertain the exact magnetic moments of individual ions.

III. GROUND STATE PROPERTIES WITH FIXED SPIN MOMENT METHOD

At first, we studied defect-free SFMO in order to demonstrate that the FSM approach is able to reproduce the correct structural ground state properties of SFMO. Therefore, as a benchmark calculation, we imposed with FSM a magnetic moment on the defect-free tetragonal SFMO unit cell and calculated the total energy in order to search for the most stable spin configuration. The configuration with a net magnetic moment (MM) of $m_{\text{gs}} = 4.0\mu_B/\text{f.u.}$ had finally the lowest total energy and is, therefore, the ground state at 0 K for defect-free unstrained SFMO. We have to note that this ground state shows directly the half-metallic density of states (DOS) with only spin down states at the Fermi energy. The additional application of correlation corrections within GGA+ U ($U = 4$ eV on Fe-3d orbitals) on

TABLE I. Structural properties of defect-free, unstrained $\text{Sr}_2\text{FeMoO}_6$ with FSM: bulk modulus B_0 , Grüneisen constant B'_0 , and the lattice parameters. The units are given in brackets, while B'_0 is dimensionless. Experimental results for polycrystalline $\text{Sr}_2\text{FeMoO}_6$ samples obtained at room temperature vary in grain size from 50 nm or 100 nm [44] to $\sim 2\mu\text{m}$ [45].

	GGA	GGA+ U	Experiment [44, 45]		
B_0 (GPa)	147.42	152.80	266 ± 3	284 ± 6	331 ± 12
B'_0	4.68	4.44	4.0	4.0	4.0
a (Å)	5.5522	5.6378	5.5703	5.5791	5.5703
c (Å)	7.9013	7.9731	7.7879	7.8698	7.8832
grain size (nm)			~ 2000	100	50

TABLE II. Single crystal elastic constants c_{ij} of defect-free, unstrained $\text{Sr}_2\text{FeMoO}_6$ with FSM written in Voigt notation and in GPa.

	c_{11}	c_{12}	c_{13}	c_{33}	c_{44}	c_{66}
GGA	230.32	77.70	108.93	244.42	45.48	63.95
GGA+ U	245.54	82.97	109.00	267.97	48.489	76.61

top of FSM leads to a wider half-metallic band gap (from 1.3 eV to 2.4 eV), while the magnetic moment at the Fe site increases from $m_{\text{Fe}} = 3.6\mu_{\text{B}}/\text{f.u.}$ to $m_{\text{Fe}} = 3.8\mu_{\text{B}}/\text{f.u.}$

Indeed, also the corresponding lattice parameters of defect-free SFMO at the ground state ($a = b = 5.55\text{Å}$ and $c = 7.90\text{Å}$) agree very well with various experimental results [11, 44–46] for the FSM method alone (Tab. I). In fact, they are the same as the lattice parameters measured at 70 K [47] ($a = 5.5521\text{Å}$ and $c = 7.9013\text{Å}$). This agreement is much better than what can be achieved by the GGA+ U method obtained earlier [19, 20, 34] (see also our results in Tab. I).

We calculated also the bulk modulus B_0 via the hydrostatic pressure but available experimental data [44, 45] is much larger than the numerical value (Tab. I). However, we note that these experimental bulk moduli were determined with polycrystalline samples and the bulk modulus decreases strongly by 65 GPa with increasing the grain size from 50 nm to 2 μm . We can interpret our theoretical *ab initio* calculation as a kind of limit to the infinite large grain size, which could then validate the bulk modulus (147 GPa to 153 GPa) obtained in our and former calculations [20]. Applying additional correlation corrections (GGA+ U) shows here only small variations ~ 5 GPa (Tab. I).

Finally, we determined the elastic tensor of the tetragonal structure by six independent single crystal elastic constants: c_{11} , c_{12} , c_{13} , c_{33} , c_{44} and c_{66} (Tab. II). Experimentally determined elastic constants were unfortunately not available, but theoretical values for other double perovskites do not deviate far from our results (Tab. II): Ba_2MgWO_6 has $c_{11} = 256.2$ GPa, $c_{12} = 85.8$ GPa, $c_{44} = 95.3$ GPa, and $B_0 = 143.1$ GPa [48]; or $\text{Sr}_2\text{CaOsO}_6$ has

$c_{11} = 331.19$ GPa, $c_{12} = 77.47$ GPa, $c_{44} = 63.35$ GPa, and $B_0 = 162.04$ GPa [49]. For GGA+ U , the c_{ij} of SFMO, except of c_{66} , vary by less than $\leq 10\%$ (Tab. II).

We conclude that the GGA and FSM method are indeed a valid tool to calculate the ground state properties for this particular magnetic material, while the additional usage of correlation corrections does not influence the ground state properties strongly or even describes them wrongly. Hence, we applied the FSM in all further calculations including biaxial strain and/or defects: (a) We set a total magnetic moment for the unit cell and calculated the structural relaxation. (b) For a set of varying magnetic moments, we defined the structure with the lowest total energy as the most stable structural and magnetic configuration with total magnetic moment m_{gs} . If needed for reasons of comparison, we will mention explicitly the use of correlation corrections (GGA+ U).

IV. VARIATIONS IN BULK SFMO WITH BIAXIAL STRAIN

In our previous study [13], only calculations at selected biaxial strain values were considered. Here in the current work, we continued with a comprehensive study of SFMO for a larger range of biaxial strain going from -10% to 10% . The structural and magnetic configuration at zero strain is represented by the tetragonal ground-state structure (Fig. 1a) as described above and the biaxial strain was applied by fixing the in-plane lattice constants ($a = b$) and relaxing the out-of-plane lattice constants (c) and the internal parameters (Fig. 2). Although a similar study was already published by Lu *et al.* [34], we present the variations of the structural and magnetic properties of SFMO with biaxial strain as the basis for the later discussion of the formation energy of point defects. In addition, we used a different numerical treatment – namely the FSM method only – while Lu *et al.* [34] used the GGA+ U method with $U = 4$ eV.

At each applied biaxial strain, we ensured the true ground-state properties using the FSM approach. We characterized the corresponding structural variation by analyzing the volume, Fe-O and Mo-O bond lengths, the different height of Sr and O ions, and the octahedra rotation angles with biaxial strain. As observed already for other oxides [35, 36], SFMO does not follow the Poisson ratio but rather its volume becomes reduced (increased) for compressive (tensile) biaxial strain (Fig. 2a). The in-plane (xy) and out-of-plane (z) Fe-O bond length (red marks in Fig. 2b, distances d_1 and d_2 in Figs. 2e and 2f), vary considerably more than the Mo-O bond lengths (black marks in Fig. 2b, distances d_3 and d_4 in Figs. 2e and 2f), while their values of 2.053 Å and 1.951 Å, respectively, for unstrained SFMO agree well with experimental values [46]. The bond lengths follow the natural tendency, the in-plane contributions become smaller with compressive biaxial strain and elongated for tensile biaxial strain, while it is vice versa for the out-of-plane bond

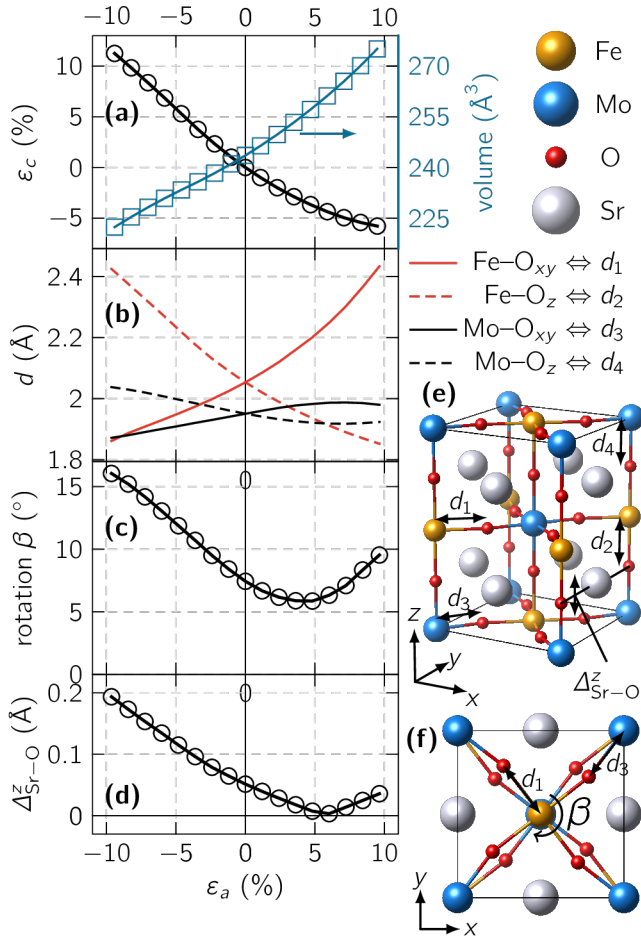


FIG. 2. (Color online) Structural variation with biaxial strain in the lattice constants $a = b$. (a) Variation of lattice parameter c and the volume of the tetragonal cell. (b) The in-plane (xy) and out-of-plane z bond lengths Mo-O and Fe-O. (c) Octahedra rotation angle β , visualized in (f). (d) Out-of-plane distances between Sr and O. (e)-(f) Visualization of distances and angles in the tetragonal unit cell.

lengths. The oxygen ions hybridize stronger with the $4d$ states of Mo than with the $3d$ states of Fe. Already Solovyev [50] found that a smaller Mo-O bond length should be the natural state of SFMO. The bond lengths are also connected with the rotation angles of the oxygen octahedra (angle β in Fig. 2f). The rotation becomes larger under compressive biaxial strain (Fig. 2c). Hence, the additional octahedra rotation is another mechanism in order to compensate the in-plane biaxial strain [35]. In z direction, the elongation caused by the compressive in-plane strain causes the oxygen ions to hybridize even stronger with Mo, while the Fe-O bond becomes much larger (Fig. 2b). The octahedra experience even stronger breathing distortions than in the ground state [50]. The other oxygen ions in the xy plane of Sr-O avoid in a similar way the compressive strain by relaxing out of that plane (Fig. 2e). Interestingly, the oxygen ions do not re-

lax closer to the Fe ions but form an ideal plane with Sr and relax out of the plane again for larger tensile strains.

These internal structural changes influence of course magnetic and electronic properties as it was observed already earlier [34]. Using only the FSM methods, we obtain only small variations for the experimental relevant range of $\pm 4\%$ biaxial strains. The Fe ions keep their high spin state with a maximal local magnetic moment of $3.63\mu_B/\text{f.u.}$ at zero strain (unstrained SFMO), which is only slightly diminished for both strains – compressive or tensile – in agreement with the conclusions of Lu *et al.* [34] (Fig. 3a). The same holds true for the antiparallely aligned magnetic moments at the Mo ions – the absolute value is slightly reduced (Fig. 3b). The local magnetic moments at the oxygen ions follow the opposite tendency of their bond lengths with the Fe and Mo ions (Fig. 2b). The local moment increases, if the bond length is reduced, and decreases, if the bond length is elongated (Fig. 3c).

The situation changes for compressive strains, which are larger than -4% . Here, we obtained a transition to a completely metallic state because the band gap in the majority spin channel $\Delta_{\uparrow}E$ closes (marked with a vertical dashed line in Fig. 3d). With the compressive biaxial strain, the Fe e_g^{\uparrow} states are almost linearly shifted towards the Fermi energy E_F (see inset in Fig. 3h and [40]). At that strain value when the Fe e_g^{\uparrow} state “hits” the Fermi energy, a kind of “jump” seems to appear. This only follows from the fact that $\Delta_{\uparrow}E$ is measured from the Fe e_g^{\uparrow} states to the Mo t_{2g}^{\uparrow} states. The position of the unoccupied Mo t_{2g}^{\uparrow} states does not change.

This result contradicts Lu *et al.* [34], who observed instead a half-metallic state with a spin transition from high spin to intermediate spin of the local moment at the Fe ion. Hence, we present also calculations with the FSM method including correlations corrections via GGA+ U (right side of Fig. 3). The combination of FSM and GGA+ U allows to determine accurately the magnetic ground state of SFMO. For compressive biaxial strain, we neither observe a spin transition nor a half-metal to metal transition (Fig. 3h). The Fe e_g^{\uparrow} states are now much further below the Fermi energy and 10% compressive strain is not enough to shift them far enough. We can only guess that the spin transition could be another local minimum in the energy landscape of SFMO, while the FSM methods ensures the correct magnetic ground state.

On the other hand, the spin transition in the tensile strain region at $\sim 5\%$ (marked with a vertical dashed line in Fig. 3h), which is as well reported by Lu *et al.* [34] for $\sim 7\%$, seems to be a stable magnetic phase transition. While the exact biaxial strain value of the transition may vary with the FSM treatment, the ferrimagnetic state becomes ferromagnetic (FIM-FM transition). The magnetic moment of Fe ions decreases from $3.95\mu_B/\text{f.u.}$ to $3.50\mu_B/\text{f.u.}$, while the Mo ions go into a low-spin state [34] and their local moments align each other parallel with the magnetic moments of the Fe ions

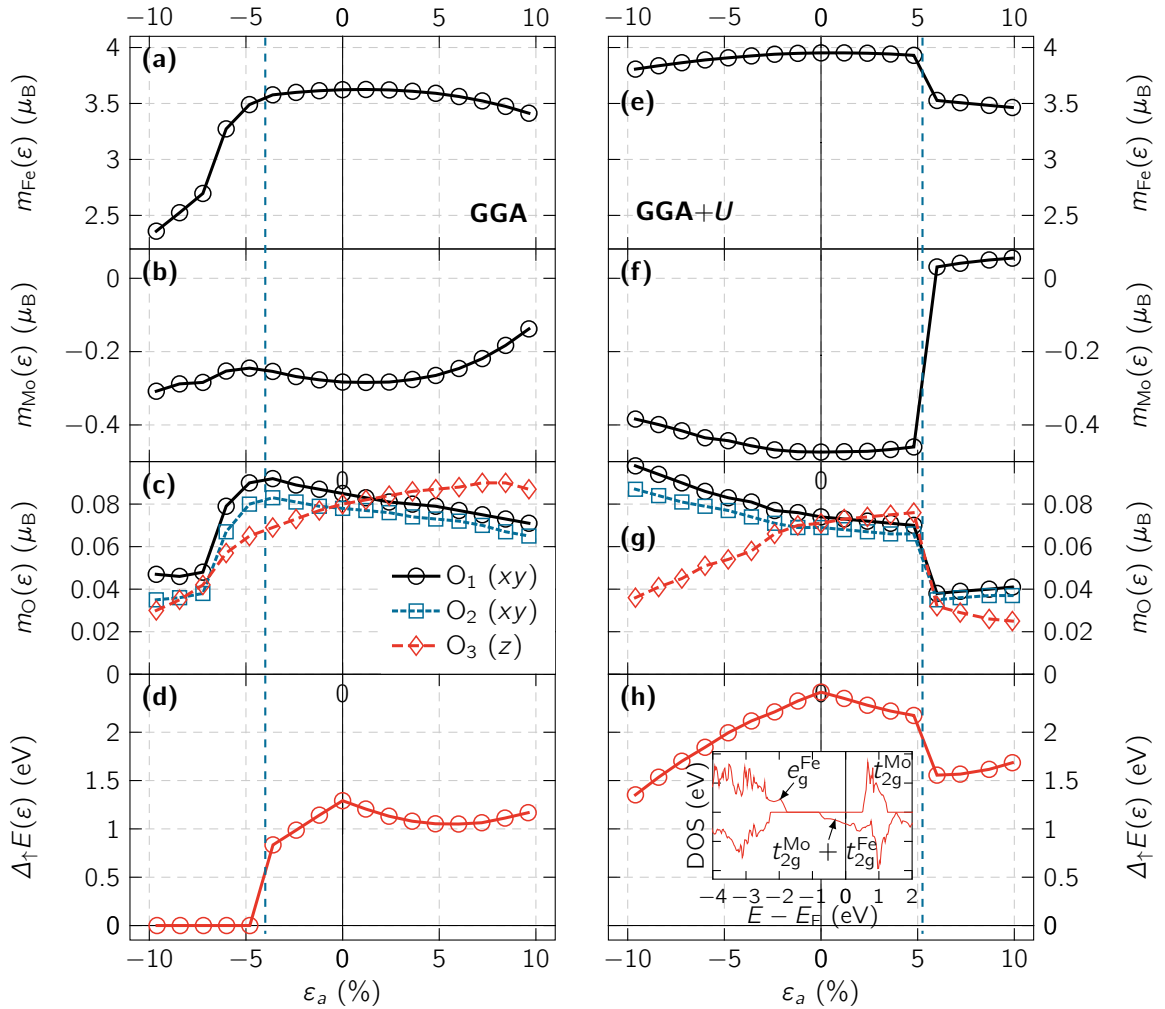


FIG. 3. (Color online) Variations of magnetic and electronic properties with biaxial strain for GGA and GGA+ U . The local magnetic moments for (a), (e) Fe ions, (b), (f) Mo ions, and (c), (g) O ions. (d), (h) Band gap in the majority spin channel calculated from the density of states (DOS). The inset shows the DOS for unstrained defect-free SFMO. The vertical dashed line at -4% on the left hand side marks the spin transition from half-metallic high-spin state to metallic low-spin state. The vertical dashed line at 5% on the right hand side marks the transition from ferrimagnetic (FIM) to ferromagnetic (FM) state.

(Fig. 3e).

Hence, we can conclude that the observed variations in the electronic and magnetic properties are rather small and not yet relevant in experimental conditions for SFMO (moderate strain values of -4% to 4%) [13]. Nevertheless, we can observe an important effect of biaxial strain for the formation of point defects demonstrated in the next section.

V. POINT DEFECTS IN SFMO WITH BIAxIAL STRAIN

Using the supercell consisting of $2 \times 2 \times 1$ tetragonal unit cells and 80 atoms (Fig. 1c), we calculated the defect formation energies of different point defects D following Nayak *et al.* [51] and considered in addition a strain ε de-

pendence as $E_{\text{form}}(D, \varepsilon)$. We briefly recall the technical details of determining the defect formation energy from the DFT total energies in the Supporting Information.

We considered besides common defect configurations such as oxygen vacancies (V_{O}) and antisite disorder (ASD) also cation vacancies of Mo (V_{Mo}), Fe (V_{Fe}), Sr (V_{Sr}), as well as non-stoichiometric disorder – a Fe ion at a Mo sublattice (Fe_{Mo}) or a Mo ion at a Fe sublattice (Mo_{Fe}). We took also into account the two nonequivalent oxygen positions, in-plane (O_{xy}) and out-of-plane (O_z) (Fig. 2), since the properties of the corresponding vacancies, $V_{\text{O}_{xy}}$ and V_{O_z} , respectively, might change considerably, as shown for CaMnO_3 [35]. We note that the absolute values of formation energies are limited to the choice of the chemical potentials μ_i , since the chemical potentials exactly suitable to the experimental growth conditions are unknown. Here, we chose the chemical

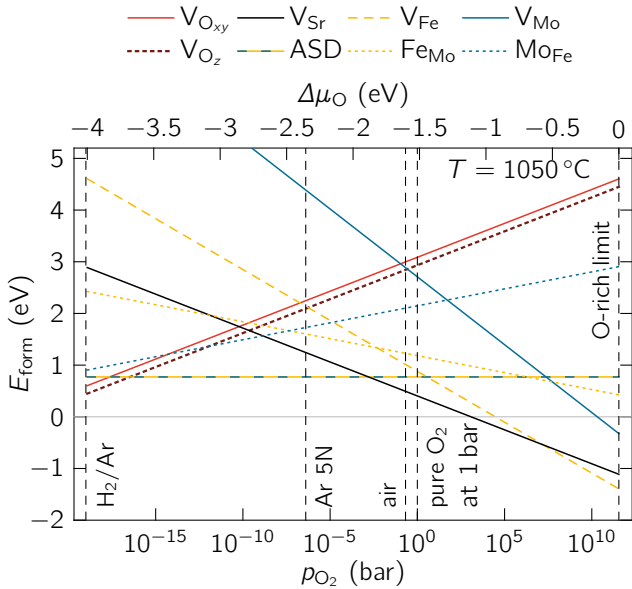


FIG. 4. (Color online) Defect formation energy of defects in unstrained SFMO ($\varepsilon = 0$) for varying oxygen partial pressure at $T = 1050$ °C. The relative chemical potential is shown at the upper axis. The legend is given above the figure.

potentials of the respective oxides for all the chemical elements in SFMO (SrO, Fe₂O₃, MoO₂) and the oxygen rich condition $\mu_{\text{O}}^{\text{max}}$ for the oxygen chemical potential [40]. In addition, the oxygen chemical potential can be varied as a parameter in order to simulate experiments at different oxygen partial pressure using thermodynamic considerations [40, 51, 52]. The results are straight lines with the slope $\propto \Delta\mu_{\text{O}} = \mu_{\text{O}} - \mu_{\text{O}}^{\text{max}}$ and $E_{\text{form}}(D, \varepsilon = 0)$ at $\Delta\mu_{\text{O}} = 0$ (Fig. 4). While the formation of metal vacancies V_{Fe} , V_{Sr} and V_{Mo} is extremely “easy” due to the negative $E_{\text{form}}(D, \varepsilon, \Delta\mu_{\text{O}} = 0)$, it is not surprising that both types of oxygen vacancies $V_{\text{O}_{xy}}$, V_{O_z} (reddish lines) are less probable in the oxygen rich regime. With less oxygen partial pressure, the formation energy of all metal vacancies increases and their appearance gets more unlikely. Just at very low partial pressures (\sim H₂/Ar atmosphere), the formation energy of oxygen vacancies becomes comparable with the one of ASD. Hence, the relative probability of point defects are very sensitive to the exact experimental conditions.

We are well aware of other choices for reference chemical potentials of multicomponent compounds using, e.g., the concept of constitutional defects developed by Hagen and Finnis for ordered alloys [53], which was applied for Sr₂FeMoO₆ [19]. There the extreme case of Mo rich (Mo_{Fe}) or Fe rich Fe_{Mo} was used as references [19], which makes a direct comparison complicated and we restrict ourselves to the comparison of the electronic structure as discussed above.

At first, we verified for strain free SFMO that GGA and FSM are applicable and we can avoid computational heavy calculations with, e.g., hybrid-functional methods,

which might raise problems for the calculations of defect formation energies or need postprocessing as discussed in [51]. In particular, the choice of a specific U for GGA+ U calculations cannot be simply transferred to any of the reference systems used to determine the formation energy. Hence, we crosschecked again the electronic structure including now the different defects in the supercell. We observe that in agreement with other theoretical studies [19, 20, 22] only in the case of oxygen, iron, or strontium vacancies, no additional states form in the spin up channel at the Fermi energy and the DOS remains half-metallic [40].

The formation energies at biaxial strains follow then by considering total energies of the relaxed supercells including defects, scaled with respect to the defect-free, ground state total energy for a series of moderate biaxial strains (-6% to $+6\%$). We note that for compressive strains $< -4\%$, the observed spin transition, discussed in the last section (Fig. 3), might cause also changes in the formation energy, which would be hard to separate from purely strain mediated effects. Different oxygen partial pressure just scales all lines by an additive term depending on the respective chemical potentials with $\Delta\mu_{\text{O}}$ or p_{O_2} (Fig. 4). Hence, we obtained that the applied biaxial strain lowers for both oxygen vacancy types – $V_{\text{O}_{xy}}$ and V_{O_z} – the formation energy and increases the probability of oxygen vacancies, with a more pronounced effect on the out-of-plane oxygen vacancy V_{O_z} (Fig. 5a). This observation is in contrast with the results obtained for, e.g., CaMnO₃ [35], but we can also expect rather different intrinsic strain relaxation mechanism in the largely distorted perovskite structure of CaMnO₃ and the less distorted SFMO structure. The latter seems to compensate the compressive strain along the z axis in the tensile regime with more oxygen vacancies in the out-of-plane direction, while it becomes opposite for larger compressive strains $\varepsilon \leq -5\%$ (maybe influenced by the spin transition). Nevertheless, we can state that the oxygen vacancy formation is easier in biaxial strained films. This will be an advantage not only for solid oxide fuel cells but also for the magnetic properties of SFMO, since we found recently that the Curie temperature can be strongly enhanced by oxygen vacancies in SFMO [37].

On the contrary, the formation energies of antisite defects increase for a large range of biaxial strain, e.g., (increase of $E_{\text{form}}(D)$) by $+386$ meV and $+78$ meV for compressive or tensile strains $\varepsilon \pm 3\%$ (Fig. 5). It only becomes reduced by -48 meV for small tensile strains in the range of $0 < \varepsilon < 3\%$ and gets again larger for tensile strains $> 2\%$. That means that, in terms of applications, biaxial strained films should be more ordered and better samples for spintronic applications [13]. This can be related to already made experimental observations on ASD. Various experiments investigated the A site substitution in double perovskites ($A_2BB'O_6$) and its influence to magnetization, spin polarization, ASD, etc. Chan *et al.* [16] found a chemical pressure in SFMO, when substituting Sr with Ca, which caused an increase in magnetic mo-

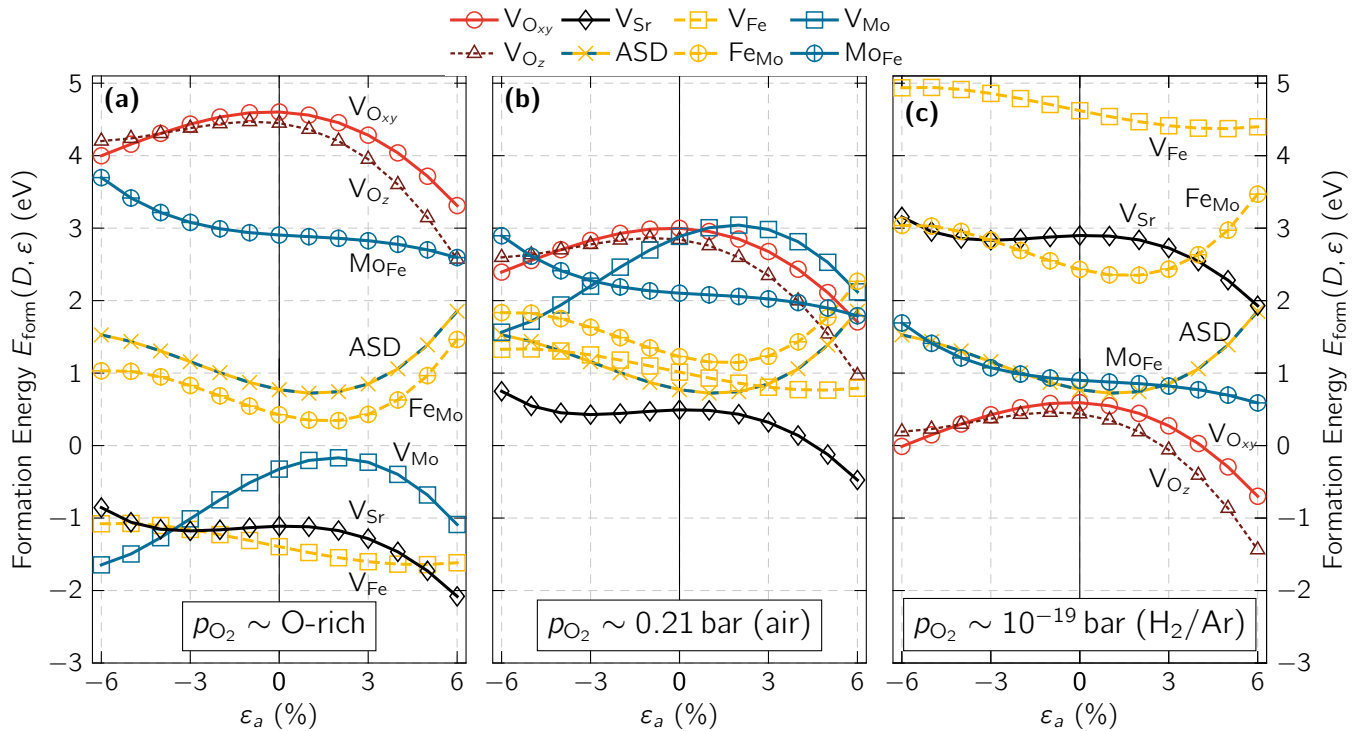


FIG. 5. (Color online) Formation energies of defects in dependence of biaxial strain and three different oxygen partial pressures. The legend is given above the figure. V_{Mo} is out of range in figure (c).

ment but also an pronounced decrease in ASD. Hence, compression can, besides the chemical variations from Sr to Ca, reduce the number of anti-site defects. Kahoul *et al.* [18] observed on the other hand an increase in the lattice constant of SFMO, when doping Sr with La, and this raised also the measured amount of ASD. Although the effects of chemical substitution could overlay effects caused by a lattice constant variation, these experiments include hints of our theoretical observations.

Considering the other defects, we found that V_{Sr} , V_{Fe} and Mo_{Fe} are less influenced by the biaxial strains -3% to 3% . Only $E_{form}(V_{Sr}, \epsilon)$ lowers considerably (-1 eV) for larger tensile strains, which then favors V_{Sr} over V_{Fe} (Fig. 5a). Moreover, ASD can be considered as a defect complex of the two non-stoichiometric defects – Mo_{Fe} and Fe_{Mo} . The average of their formation energies taking into account the oxygen chemical potential properly matches the one of the antisite defects. The high formation energy of Mo_{Fe} is however surprising, because we would expect substitution of Fe with Mo much more likely, since $SrMoO_x$ is a typical impurity phase when growing SFMO films [54, 55].

This discrepancy is resolved when we consider lower oxygen partial pressures, e.g., at ambient air pressure (Fig. 5b) or almost vacuum (Fig. 5c). Not only become V_{Oxy} more and V_{Mo} less likely, also all formation energies shift to positive formation energies at $\epsilon = 0$. The latter means that there are no spontaneous vacancies anymore and SFMO is indeed stable. Only at large tensile strains,

$E_{form}(V_{Sr})$ still gets below zero. This means that biaxial strains can significantly alter the energy landscape – the relative order of the defect formation energies or their crossing points (better visible in Fig. 4). The low $E_{form}(V_{Sr})$ also means that V_{Sr} are very likely to appear in SFMO for a large range of experimental conditions. Therefore, Sr vacancies could be more important than earlier expected and might also deteriorate the magnetic properties of SFMO [56]. Also the formation of Mo oxide impurity phases is more likely at ambient air partial pressure – Fe vacancies form easily and can be filled by Mo (Mo_{Fe}).

When going to lower partial pressures, antisite defects become the most likely defect (Figs. 4 and 5b) and only for partial pressures smaller than 10^{-16} bar oxygen vacancies will be the most probable defect type (Fig. 5c). Then, non-stoichiometric Mo at an Fe site has an almost similar probability to form than an antisite defect. This means that $SrMoO_x$ impurity phases are even more likely close to vacuum.

VI. CONCLUSIONS

We showed that realistic biaxial strains will have a pronounced effect on the point defect profile of oxide materials – here Sr_2FeMoO_6 – via a strong influence on the defect stability ($E_{form}(D, \epsilon)$ varies by ~ 0.2 eV per 1% strain). The half-metallic ground state of defect-free

SFMO will be preserved at moderate strains, but the relative order of formation energies for different defects might be altered, e.g., V_{Fe} vs. V_{Sr} ; or $V_{\text{O}_{xy}}$ vs. V_{O_z} .

Most interestingly, the amount of antisite defect formation can be reduced in compressively strained SFMO films and oxygen vacancies will form much easier under both strains – compressive and tensile. Latter defects are crucial for solid oxide fuel cells or can enhance magnetic properties in SFMO [13, 37].

Taking into account also the oxygen partial pressure as an experimental parameter offers another degree of freedom for the defect formation energies. Our numerical results at partial pressures matching air or vacuum atmosphere can be compared directly with experimental

measurements. We found that V_{Sr} are very likely over a large range of partial pressures, while oxygen vacancies become most likely only for very low partial pressures $< 10^{-16}$ bar. Hence, we have demonstrated the potential of targeted first-principles calculations in designing strain-defect engineering processes for the tuning of the properties of SFMO or other oxides.

ACKNOWLEDGMENTS

This publication was funded by the German Research Foundation within the Collaborative Research Centre 762 (projects A4 and B1).

-
- [1] R. P. Panguluri, S. Xu, Y. Moritomo, I. V. Solovyev, and B. Nadgorny, *Appl. Phys. Lett.* **94**, 012501 (2009).
- [2] M. Bibes, K. Bouzehouane, A. Barthélémy, M. Besse, S. Fusil, M. Bowen, P. Seneor, J. Carrey, V. Cros, A. Vaurès, J.-P. Contour, and A. Fert, *Appl. Phys. Lett.* **83**, 2629 (2003).
- [3] A. Nag, S. Jana, S. Middey, and S. Ray, *Indian J. Phys.* **91**, 883 (2017).
- [4] J. Fontcuberta, D. Rubi, C. Frontera, J. L. García-Muñoz, M. Wojcik, E. Jedryka, S. Nadolski, M. Izquierdo, J. Avila, and M. C. Asensio, *J. Magn. Magn. Mater.* **290-291 PA**, 974 (2005).
- [5] H. Q. Yin, J. S. Zhou, J. P. Zhou, R. Dass, J. T. McDevitt, and J. B. Goodenough, *Appl. Phys. Lett.* **75**, 2812 (1999).
- [6] T. Manako, M. Izumi, Y. Konishi, K.-I. Kobayashi, M. Kawasaki, and Y. Tokura, *Appl. Phys. Lett.* **74**, 2215 (1999).
- [7] Y. Tomioka, T. Okuda, Y. Okimoto, R. Kumai, K.-I. Kobayashi, and Y. Tokura, *Phys. Rev. B* **61**, 422 (2000), 0001398.
- [8] A. Di Troilo, R. Larciprete, A. M. Testa, D. Fiorani, P. Imperatori, S. Turchini, and N. Zema, *J. Appl. Phys.* **100**, 013907 (2006).
- [9] K.-I. Kobayashi, T. Kimura, H. Sawada, K. Terakura, and Y. Tokura, *Nature* **395**, 677 (1998).
- [10] H. Jalili, N. F. Heinig, and K. T. Leung, *Phys. Rev. B* **79**, 174427 (2009).
- [11] M. Saloaro, S. Majumdar, H. Huhtinen, and P. Paturi, *EPJ Web. Conf.* **40**, 15012 (2013).
- [12] I. Angervo, M. Saloaro, H. Palonen, S. Majumdar, H. Huhtinen, and P. Paturi, *Phys. Procedia* **75**, 1011 (2015).
- [13] M. Saloaro, M. Hoffmann, W. A. Adeagbo, S. Granroth, H. Deniz, H. Palonen, H. Huhtinen, S. Majumdar, P. Laukkanen, W. Hergert, A. Ernst, and P. Paturi, *ACS Appl. Mater. Interfaces* **8**, 20440 (2016).
- [14] A. S. Ogale, S. B. Ogale, R. Ramesh, and T. Venkatesan, *Appl. Phys. Lett.* **75**, 537 (1999).
- [15] J. Navarro, L. Balcells, F. Sandiumenge, M. Bibes, A. Roig, B. Martínez, and J. Fontcuberta, *J. Phys.: Condens. Matter* **13**, 8481 (2001).
- [16] T. S. Chan, R. S. Liu, G. Y. Guo, S. F. Hu, J. G. Lin, J. M. Chen, and J. P. Attfield, *Chem. Mater.* **15**, 425 (2003).
- [17] S. Colis, D. Stoeffler, C. Mény, T. Fix, C. Leuvrey, G. Pourroy, A. Dinia, and P. Panissod, *J. Appl. Phys.* **98**, 033905 (2005).
- [18] A. Kahoul, A. Azizi, S. Colis, D. Stoeffler, R. Moubah, G. Schmerber, C. Leuvrey, and A. Dinia, *J. Appl. Phys.* **104**, 123903 (2008).
- [19] R. Mishra, O. D. Restrepo, P. M. Woodward, and W. Windl, *Chem. Mater.* **22**, 6092 (2010).
- [20] A. B. Muñoz-García, M. Pavone, and E. A. Carter, *Chem. Mater.* **23**, 4525 (2011).
- [21] D. Stoeffler and S. Colis, *J. Magn. Magn. Mater.* **290-291**, 400 (2005).
- [22] Y. Zhang, V. Ji, and K.-W. Xu, *J. Alloys Comp.* **648**, 374 (2015).
- [23] A. M. Reyes, Y. Arredondo, and O. Navarro, *J. Phys. Chem. C* **120**, 4048 (2016).
- [24] J. Töpfer, R. Kircheisen, and S. Barth, *J. Appl. Phys.* **105**, 07D712 (2009).
- [25] H. Deniz, D. Preziosi, M. Alexe, and D. Hesse, *J. Appl. Phys.* **121**, 023906 (2017).
- [26] D. Serrate, J. M. D. Teresa, and M. R. Ibarra, *J. Phys.: Condens. Matter* **19**, 023201 (2007).
- [27] O. Erten, O. N. Meetei, A. Mukherjee, M. Randeria, N. Trivedi, and P. Woodward, *Phys. Rev. B* **87**, 165105 (2013), arXiv:1210.6689.
- [28] S. Y. Gómez and D. Hotza, *Renew. Sust. Energ. Rev.* **61**, 155 (2016).
- [29] H. Li, Y. Zhao, Y. Wang, and Y. Li, *Catal. Today* **259**, 417 (2016).
- [30] G. Miao, C. Yuan, T. Chen, Y. Zhou, W. Zhan, and S. Wang, *Int. J. Hydrogen Energy* **41**, 1104 (2016).
- [31] A. B. Muñoz-García, A. M. Ritzmann, M. Pavone, J. A. Keith, and E. A. Carter, *Acc. Chem. Res.* **47**, 3340 (2014).
- [32] L. V. Kovalev, M. V. Yarmolich, M. L. Petrova, J. Us-tarroz, H. A. Terryn, N. A. Kalanda, and M. L. Zheludkevich, *ACS Appl. Mater. Interfaces* **6**, 19201 (2014).
- [33] T. Fix, D. Stoeffler, S. Colis, C. Ullhaq, G. Versini, J. P. Vola, F. Huber, A. Dinia, C. Ullhaq, G. Versini, J. P. Vola, F. Huber, and A. Dinia, *J. Appl. Phys.* **98**, 023712 (2005).
- [34] R. Lu, H. Wu, Y. Qian, E. Kan, Y. Liu, W. Tan, C. Xiao, and K. Deng, *Solid State Commun.* **191**, 70 (2014).

- [35] U. Aschauer, R. Pfenninger, S. M. Selbach, T. Grande, and N. A. Spaldin, *Phys. Rev. B* **88**, 054111 (2013).
- [36] U. Aschauer, N. Vonrüti, and N. A. Spaldin, *Phys. Rev. B* **92**, 054103 (2015).
- [37] M. Hoffmann, V. N. Antonov, L. V. Bekenov, K. Kokko, W. Hergert, and A. Ernst, ArXiv:1504.02629 (2015), arXiv:1504.02629.
- [38] G. Kresse and J. Hafner, *Phys. Rev. B* **47**, 558 (1993).
- [39] G. Kresse and J. Furthmüller, *Comp. Mater. Sci.* **6**, 15 (1996).
- [40] See Supplemental Material below for details about the computational setup, the electronic structure of SFMO, and the calculation of defect formation energies.
- [41] K. Schwarz and P. Mohn, *J. Phys. F: Met. Phys.* **14**, L129 (1984).
- [42] P. M. Marcus and V. L. Moruzzi, *J. Appl. Phys.* **63**, 4045 (1988).
- [43] T. Saitoh, M. Nakatake, A. Kakizaki, H. Nakajima, O. Morimoto, S. Xu, Y. Moritomo, N. Hamada, and Y. Aiura, *Phys. Rev. B* **66**, 035112 (2002).
- [44] P. E. J. S. Zhang, L. D. Yao, F. Y. Li, Z. X. Bao, J. X. Li, Y. C. Li, J. Liu, C. Q. Jin, and R. C. Yu, *J. Mater. Sci.* **41**, 7374 (2006).
- [45] P. Zhao, R. C. Yu, F. Y. Li, Z. X. Liu, M. Z. Jin, and C. Q. Jin, *J. Appl. Phys.* **92**, 1942 (2002).
- [46] D. D. Taylor, N. J. Schreiber, C. M. Brown, A. M. Arevalo-Lopez, and E. E. Rodriguez, *Chem. Comm.* **51**, 12201 (2015).
- [47] O. Chmaissem, R. Kruk, B. Dabrowski, D. E. Brown, X. Xiong, S. Kolesnik, J. D. Jorgensen, and C. W. Kimball, *Phys. Rev. B* **62**, 14197 (2000).
- [48] L. Shi, L. Wu, Y. F. Duan, J. Hu, X. Q. Yang, G. Tang, and L. Z. Hao, *Eur. Phys. J. B* **86**, 9 (2013).
- [49] M. Faizan, G. Murtaza, S. H. Khan, A. Khan, A. Mehmood, R. Khenata, and S. Hussain, *Bull. Mater. Sci.* **39**, 1419 (2016).
- [50] I. V. Solovyev, *Phys. Rev. B* **65**, 144446 (2002).
- [51] S. K. Nayak, H. T. Langhammer, W. A. Adeagbo, W. Hergert, T. Müller, and R. Böttcher, *Phys. Rev. B* **91**, 155105 (2015).
- [52] K. Reuter and M. Scheffler, *Phys. Rev. B* **65**, 035406 (2001).
- [53] M. Hagen and M. W. Finnis, *Philos. Mag. A* **77**, 447 (1998).
- [54] J. Santiso, A. Figueras, and J. Fraxedas, *Surf. Interface Anal.* **33**, 676 (2002).
- [55] J. Raittila, T. Salminen, T. Suominen, K. Schlesier, and P. Paturi, *J. Phys. Chem. Solids* **67**, 1712 (2006).
- [56] L. Harnagea and P. Berthet, *J. Solid State Chem.* **222**, 115 (2015).

Supplemental Material:
Tuning the probability of defect formation via substrate strains in
 $\text{Sr}_2\text{FeMoO}_6$ films

Waheed A. Adeagbo,¹ Martin Hoffmann,² Arthur Ernst,^{2,3} Wolfram Hergert,¹ Minnamari Saloaro,⁴ Petriina Paturi,⁴ and Kalevi Kokko^{5,6}

¹*Institute of Physics, Martin Luther University Halle-Wittenberg,
Von-Seckendorff-Platz 1, 06120 Halle, Germany**

²*Institute for Theoretical Physics, Johannes Kepler
University Linz, Altenberger Straße 69, 4040 Linz, Austria[†]*

³*Max Planck Institute of Microstructure Physics, Weinberg 2, 06120 Halle, Germany*

⁴*Wihuri Physical Laboratory, Department of Physics and
Astronomy, University of Turku, FI-20014 Turku, Finland*

⁵*Department of Physics and Astronomy, University of Turku, FIN-20014 Turku, Finland*

⁶*Turku University Centre for Materials and Surfaces (MatSurf), Turku, Finland*

* waheed.adeagbo@physik.uni-halle.de

† martin.hoffmann@jku.at

A. VASP parameters

As exchange correlation functional, we used the generalized gradient approximation given in the Perdew-Burke-Ernzerhof (PBE) [1] form shortly noted as GGA. The projector augmented-wave (PAW) [2] method chosen for the treatment of core electrons yields a better ground state structure for oxide materials. The plane-wave expansion of the electronic wavefunctions was cut-off at the kinetic energy of 400 eV. The internal parameters and the lattice parameter c were allowed to relax using the conjugate gradient algorithm until the forces were smaller than the tolerance value of 0.001 eV/Å. Atomic coordinates in tetragonal unit cell as a result of structural relaxation are given in Tab. I. We used a \mathbf{k} -point mesh of $8 \times 8 \times 6$ within the Monkhorst-Pack special \mathbf{k} -point scheme for the tetragonal cell and a $4 \times 4 \times 6$ \mathbf{k} -point mesh for the supercell to span the irreducible Brillouin zone [3] (see structures in Figure 1 of the main manuscript).

We calculated the elastic tensor for Sr₂FeMoO₆ (SFMO) from evaluations of the stress tensor generated by small strains [4].

B. Density of States in defect-free Sr₂FeMoO₆

As shown already in many other theoretical papers, the density of states of SFMO reveals a half-metallic state (Fig. 1). However, the appearance of the band gap in the spin up channel in the numerical calculations is very sensitive to the particular numerical framework: One of the first calculations for example simply obtained half-metallic density of states [5]. On the other hand, the microstructure and the position of the oxygen ions with respect to the Fe and Mo ions seems to be crucial for the spin up band gap [6]. Lately, adding correlation corrections via DFT+ U approaches are named as the right tool in order to obtain half-metallicity [7–9]. Using the fixed spin moment approach and a generalized gradient approximation (GGA) exchange-correlation functional only, we obtained the half-metallic ground state with a total magnetic moment of $4\mu_B$ /f.u.. The structural properties resemble very well experimental findings as discussed in the main manuscript.

Here, we want to emphasize on the density of states. The spin up band gap is for defect-free, unstrained SFMO 1.3 eV, measured between the unoccupied Mo t_{2g}^\uparrow and the occupied Fe e_g^\uparrow (Fig. 1). The position of the unoccupied Mo t_{2g}^\uparrow explains also the "jump" of the spin

TABLE I. Structural relaxation of the tetragonal unit cell of unstrained SFMO ($\varepsilon = 0$) with FSM method and PBE functional. Lattice constants are $a = b = 5.5522 \text{ \AA}$ and $c = 7.9013 \text{ \AA}$. Internal positions are scaled with the respective lattice constants.

site	x	y	z
Sr	0	1/2	1/4
Sr	0	1/2	3/4
Sr	1/2	0	1/4
Sr	1/2	0	3/4
Fe	0	0	1/2
Fe	1/2	1/2	0
Mo	0	0	0
Mo	1/2	1/2	1/2
O	0.210 31	0.278 68	0
O	0.789 69	0.721 32	0
O	0.721 32	0.210 31	0
O	0.278 68	0.789 69	0
O	0.710 31	0.778 68	1/2
O	0.289 69	0.221 32	1/2
O	0.221 32	0.710 30	1/2
O	0.778 68	0.289 69	1/2
O	0	0	0.244 98
O	0	0	0.755 02
O	1/2	1/2	0.744 98
O	1/2	1/2	0.255 02

up band gap described in the main manuscript. In the spin down channel, the Mo t_{2g}^{\downarrow} and Fe t_{2g}^{\downarrow} hybridize creating states at the Fermi energy. Applying an Hubbard U of 4 eV shifts the Fe e_g^{\uparrow} downwards and increases the spin up band gap to 2.4 eV. This is of the same order as obtained by earlier calculations [8, 9], although the value is given as ~ 1.9 eV by Lu *et al.*

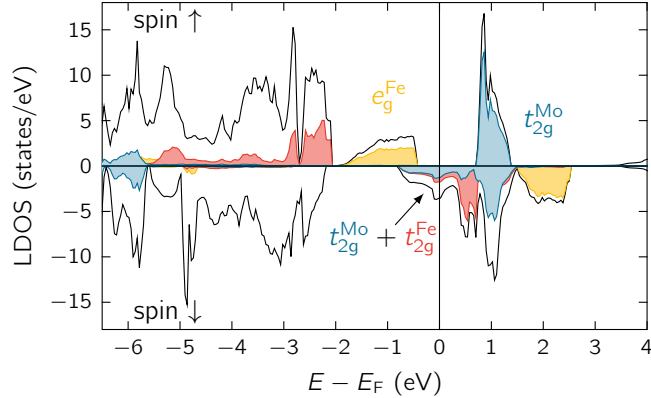


FIG. 1. Spin-resolved local density of states (LDOS) of unstrained and defect-free SFMO calculated with VASP.

citeLu2014ssc (the value seems to be counted only until the Fermi energy).

Although the spin up band gap in our case is rather small in comparison with other reports, the comparison with experimental values (0.5 eV, 1.3 eV) shows a good agreement [10, 11]. The first one represents an optical measurement, while the second experimental band gap follows from photoemission spectroscopy. Of course, we have to consider also a thermal broadening of the electronic states with increasing temperature when comparing the size of the theoretical and experimental band gap.

C. Electronic Properties of Point Defects in SFMO

Now, we consider also point defects in SFMO and calculate the band gap (Tab. II). As in the defect-free case, the Fe- e_g^\uparrow states become more localized with GGA+ U and an already existing spin up band gap only widens by roughly 1 eV (Tab. II). Only for the non-stoichiometric defect Fe_{Mo} (additional Fe at a Mo site), a spin up band gap opens within the GGA+ U , because the states of the additional Fe_{Mo} become more localized.

D. Formation Energy

The formation energies provide a way to map the ground-state DFT calculations to the thermodynamic conditions accessible in experiment, and the relative comparison helps in judging the relative stability of various defects at a given environmental condition. We

TABLE II. Half metallic band gaps ($\Delta_{\uparrow}E$) of unstrained SFMO ($\varepsilon = 0$) including defects.

configurations	$\Delta_{\uparrow}E$ (eV)	
	GGA	GGA+ U
defect-free	1.3	2.4
ASD	0.0	0.0
$V_{O_{xy}}, V_{O_z}$	1.1	2.3
V_{Mo}	0.0	0.0
V_{Fe}	1.2	2.2
V_{Sr}	1.3	2.2
Fe_{Mo}	0.0	2.0
Mo_{Fe}	0.0	0.0

calculated the formation energies in dependence of strain as [12]

$$E_{\text{form}}(D, \varepsilon) = E(D, \varepsilon, q = 0) - E_{\text{Host}}(\varepsilon) + \sum_i p_i n_i \mu_i. \quad (1)$$

Therein, $E(D, \varepsilon, q = 0)$ and $E_{\text{host}}(\varepsilon)$ are the calculated total energies of the supercell including defect (D), which is uncharged ($q = 0$, notation dropped in the following), and the host supercell of equal size under the influence of the strain ε , respectively. Equation (1) is balanced using the chemical potentials (μ_i) of the elemental species (i). Since the energy dependence of the chemical potentials with strain was negligibly small compared with the difference between the total energies of strained bulk elements and their respective equilibrium structure (below 0.2 eV), we approximated the chemical potentials as strain independent. Their variations were not affecting the overall trend of the formation energies. In Equation (1), the number of defects is n_i and the factor p_i is either -1 or $+1$ for atoms added to or removed from the host supercell in the process of constructing the defect supercells [12, 13].

We took the chemical potentials used in (1) from the respective oxides of all the constituent metal elements. This means the total energy of SrO in the NaCl structure by

$$\mu_{\text{Sr}} + \mu_{\text{O}} = E(\text{SrO}). \quad (2)$$

and of Fe_2O_3 and MoO_2 ground state bulk phase for μ_{Fe} and μ_{Mo} , respectively. The chemical potentials of oxygen μ_{O} was derived from half of the total energy of the oxygen molecule in

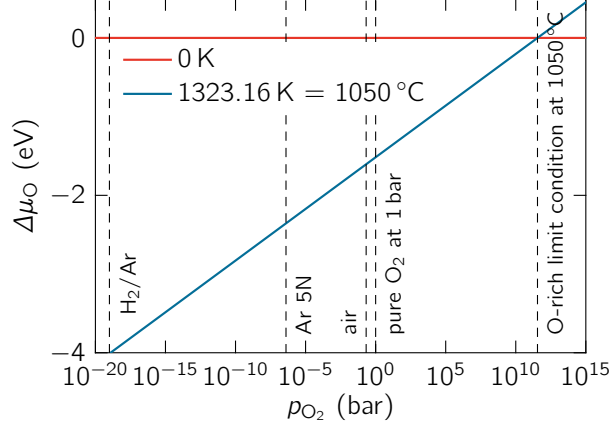


FIG. 2. Relation between oxygen partial pressure (p_{O_2}) and the relative chemical potential of oxygen ($\Delta\mu_{\text{O}}$) at $T = 0\text{ K}$ and 1050 °C . The estimation is done by using (4) together with the absolute value for the oxygen chemical potential at O-rich condition set to zero [12].

the same volume as the supercell, i.e.,

$$\mu_{\text{O}}^{\text{max}} = \frac{1}{2}E(\text{O}_2) = -4.916\text{ eV}, \quad (3)$$

which is considered as the oxygen rich limit.

However, the extremely rich case is not realized in experiments and the respective oxygen chemical potential will be reduced at experimental conditions. This can be seen from the thermodynamic relation between the oxygen chemical potential and the oxygen partial pressure (p_{O_2}) at a given temperature following the idea of Refs. [12, 14]

$$\mu(T, p_{\text{O}_2}) = \mu_{\text{O}}(T, p^\circ) + \frac{1}{2}kT \ln\left(\frac{p_{\text{O}_2}}{p^\circ}\right), \quad (4)$$

where p° is the standard pressure of 1 bar. The values of $\mu_{\text{O}}(T, p^\circ)$ are calculated from the entropy and enthalpy of a oxygen molecule [14]

$$\mu_{\text{O}}(T, p^\circ) = \frac{1}{2}[H(T, p^\circ, \text{O}_2) - H(0\text{ K}, p^\circ, \text{O}_2)] - \frac{1}{2}T[S(T, p^\circ, \text{O}_2) - S(0\text{ K}, p^\circ, \text{O}_2)]. \quad (5)$$

Both quantities are listed in NIST-JANAF thermochemical tables [15]. In order to link the value of μ_{O} in Eq. (3) to the thermodynamic expression of Eq. (4), we choose a common reference $\mu_{\text{O}}(0\text{ K}, p) = \mu_{\text{O}}^{\text{max}}$ and defined the variation of the chemical potential as $\Delta\mu_{\text{O}}(T, p) = \mu_{\text{O}}(T, p) - \mu_{\text{O}}^{\text{max}}$, which becomes $\Delta\mu_{\text{O}}(0\text{ K}, p) = 0\text{ eV}$ (Fig. 2). Finally, we assumed a temperature of $T = 1323.16\text{ K} = 1050\text{ °C}$, which is typically used when growing

epitaxial SFMO films [16–18]. We derived for $\mu_{\text{O}}(T, p^{\circ}) = -1.51627 \text{ eV}$ from the linear interpolation of equation (5) between 1300 K to 1400 K (Fig. 2).

With these equation, we could express the formation energy of the defects as a function of the oxygen partial pressure at different temperatures and obtained following equations

$$E_{\text{form}}(\text{V}_{\text{O}}, \varepsilon) = E(\text{V}_{\text{O}}, \varepsilon) - E_{\text{Host}}(\varepsilon) + (\Delta\mu_{\text{O}} + \mu_{\text{O}}^{\text{max}}), \quad (6)$$

$$E_{\text{form}}(\text{V}_{\text{Sr}}, \varepsilon) = E(\text{V}_{\text{Sr}}, \varepsilon) - E_{\text{Host}}(\varepsilon) + [E(\text{SrO}) - (\Delta\mu_{\text{O}} + \mu_{\text{O}}^{\text{max}})], \quad (7)$$

$$E_{\text{form}}(\text{V}_{\text{Fe}}, \varepsilon) = E(\text{V}_{\text{Fe}}, \varepsilon) - E_{\text{Host}}(\varepsilon) + \left[\frac{1}{2}E(\text{Fe}_2\text{O}_3) - \frac{3}{2}(\Delta\mu_{\text{O}} + \mu_{\text{O}}^{\text{max}}) \right], \quad (8)$$

$$E_{\text{form}}(\text{V}_{\text{Mo}}, \varepsilon) = E(\text{V}_{\text{Mo}}, \varepsilon) - E_{\text{Host}}(\varepsilon) + [E(\text{MoO}_2) - 2(\Delta\mu_{\text{O}} + \mu_{\text{O}}^{\text{max}})], \quad (9)$$

$$E_{\text{form}}(\text{Fe}_{\text{Mo}}, \varepsilon) = E(\text{Fe}_{\text{Mo}}, \varepsilon) - E_{\text{Host}}(\varepsilon) + [E(\text{MoO}_2) - 2(\Delta\mu_{\text{O}} + \mu_{\text{O}}^{\text{max}})] - \left[\frac{1}{2}E(\text{Fe}_2\text{O}_3) - \frac{3}{2}(\Delta\mu_{\text{O}} + \mu_{\text{O}}^{\text{max}}) \right], \quad (10)$$

$$= E(\text{Fe}_{\text{Mo}}, \varepsilon) - E_{\text{Host}}(\varepsilon) + E(\text{MoO}_2) - \frac{1}{2}E(\text{Fe}_2\text{O}_3) - \frac{1}{2}(\Delta\mu_{\text{O}} + \mu_{\text{O}}^{\text{max}}), \quad (11)$$

$$E_{\text{form}}(\text{Mo}_{\text{Fe}}, \varepsilon) = E(\text{Mo}_{\text{Fe}}, \varepsilon) - E_{\text{Host}}(\varepsilon) - [E(\text{MoO}_2) - 2(\Delta\mu_{\text{O}} + \mu_{\text{O}}^{\text{max}})] + \left[\frac{1}{2}E(\text{Fe}_2\text{O}_3) - \frac{3}{2}(\Delta\mu_{\text{O}} + \mu_{\text{O}}^{\text{max}}) \right], \quad (12)$$

$$= E(\text{Mo}_{\text{Fe}}, \varepsilon) - E_{\text{Host}}(\varepsilon) - E(\text{MoO}_2) + \frac{1}{2}E(\text{Fe}_2\text{O}_3) + \frac{1}{2}(\Delta\mu_{\text{O}} + \mu_{\text{O}}^{\text{max}}), \quad (13)$$

while stoichiometric defects remain constant

$$E_{\text{form}}(\text{ASD}, \varepsilon) = E(\text{ASD}, \varepsilon) - E_{\text{Host}}(\varepsilon). \quad (14)$$

-
- [1] J. P. Perdew, K. Burke, and M. Ernzerhof, *Phys. Rev. Lett.* **77**, 3865 (1996).
- [2] P. E. Blöchl, *Phys. Rev. B* **50**, 17953 (1994).
- [3] H. J. Monkhorst and J. D. Pack, *Phys. Rev. B* **13**, 5188 (1976).
- [4] M. J. Mehl, J. E. Osburn, D. A. Papaconstantopoulos, and B. M. Klein, *Phys. Rev. B* **41**, 10311 (1990).
- [5] K.-I. Kobayashi, T. Kimura, H. Sawada, K. Terakura, and Y. Tokura, *Nature* **395**, 677 (1998).
- [6] I. V. Solovyev, *Phys. Rev. B* **65**, 144446 (2002).
- [7] D. Stoeffler and S. Colis, *J. Magn. Magn. Mater.* **290-291**, 400 (2005).
- [8] A. B. Muñoz-García, M. Pavone, and E. A. Carter, *Chem. Mater.* **23**, 4525 (2011).

- [9] R. Lu, H. Wu, Y. Qian, E. Kan, Y. Liu, W. Tan, C. Xiao, and K. Deng, *Solid State Commun.* **191**, 70 (2014).
- [10] Y. Tomioka, T. Okuda, Y. Okimoto, R. Kumai, K.-I. Kobayashi, and Y. Tokura, *Phys. Rev. B* **61**, 422 (2000), 0001398.
- [11] T. Saitoh, M. Nakatake, A. Kakizaki, H. Nakajima, O. Morimoto, S. Xu, Y. Moritomo, N. Hamada, and Y. Aiura, *Phys. Rev. B* **66**, 035112 (2002).
- [12] S. K. Nayak, H. T. Langhammer, W. A. Adeagbo, W. Hergert, T. Müller, and R. Böttcher, *Phys. Rev. B* **91**, 155105 (2015).
- [13] C. G. Van de Walle and J. Neugebauer, *J. Appl. Phys.* **95**, 3851 (2004).
- [14] K. Reuter and M. Scheffler, *Phys. Rev. B* **65**, 035406 (2001).
- [15] M. W. Chase, Jr., *Journal of Physical and Chemical Reference Data, Monograph 9*, 4th ed. (American Institute of Physics, Washington, DC, 1998) p. 1952.
- [16] T. Manako, M. Izumi, Y. Konishi, K.-I. Kobayashi, M. Kawasaki, and Y. Tokura, *Appl. Phys. Lett.* **74**, 2215 (1999).
- [17] S. Wang, H. Pan, X. Zhang, G. Lian, and G. Xiong, *Appl. Phys. Lett.* **88**, 121912 (2006).
- [18] M. Saloaro, S. Majumdar, H. Huhtinen, and P. Paturi, *EPJ Web. Conf.* **40**, 15012 (2013).